

# **Geophysical Research Letters**\*

# <del>-</del>

# **RESEARCH LETTER**

10.1029/2023GL103002

#### **Key Points:**

- The Madden-Julian Oscillation (MJO) behaves as a moisture mode only over the Indian Ocean and is otherwise more accurately defined as a mixed moisture-gravity wave
- In this basin, the MJO is slow enough to allow for weak temperature gradient (WTG) balance and for moisture to govern convection evolution
- Otherwise, results suggest that moisture and temperature play comparable roles in the MJO's thermodynamics

#### **Supporting Information:**

Supporting Information may be found in the online version of this article.

#### Correspondence to:

V. C. Mayta, mayta@wisc.edu

#### Citation:

Mayta, V. C., & Adames Corraliza, Á. F. (2023). Is the Madden-Julian Oscillation a moisture mode? *Geophysical Research Letters*, 50, e2023GL103002. https://doi.org/10.1029/2023GL103002

Received 7 FEB 2023 Accepted 15 JUL 2023

#### **Author Contributions:**

Conceptualization: Víctor C. Mayta, Ángel F. Adames Corraliza Formal analysis: Víctor C. Mayta, Ángel F. Adames Corraliza Supervision: Víctor C. Mayta, Ángel F. Adames Corraliza Writing – review & editing: Víctor C. Mayta, Ángel F. Adames Corraliza

© 2023. The Authors.

This is an open access article under the terms of the Creative Commons Attribution License, which permits use, distribution and reproduction in any medium, provided the original work is properly cited.

# Is the Madden-Julian Oscillation a Moisture Mode?

Víctor C. Mayta<sup>1</sup> and Ángel F. Adames Corraliza<sup>1</sup>

<sup>1</sup>Department of Atmospheric and Oceanic Sciences, University of Wisconsin, Madison, WI, USA

**Abstract** The governing thermodynamics of the Madden-Julian Oscillation (MJO) is examined using sounding and reanalysis data. On the basis of four objective criteria, results suggest that the MJO behaves like a moisture mode–a system whose thermodynamics is governed by moisture–only over the Indian Ocean. Over this basin, the MJO shows a slow convective adjustment timescale, its zonal scale is smaller, and it exhibits slow propagation, allowing moisture modes to exist. Elsewhere, the faster-propagating wavenumber 1–2 components are more prominent preventing weak temperature gradient (WTG) balance to be established. As a result, temperature and moisture play similar roles in the MJO's thermodynamics outside the Indian Ocean.

**Plain Language Summary** The Madden-Julian Oscillation is one of the most important phenomena that occur at the subseasonal to seasonal timescale and is a source of weather predictability at this timescale. Despite its importance, many features of Madden-Julian Oscillation (MJO) remain elusive, and many theories have been proposed to understand its behavior. Arguably, the most recent popular MJO theory is the moisture mode theory. The theory posits that moisture governs the evolution of the MJO. Here, we show that this theory is applicable only over the Indian Ocean, where MJO's small zonal scale and slow propagation allow moisture modes to exist at the scale of the MJO. Elsewhere, temperature fluctuations in the MJO become as important as moisture, a feature that is inconsistent with the moisture mode theory.

#### 1. Introduction

The Madden-Julian oscillation (MJO) is the dominant and most well-known mode of intraseasonal variability over the tropics (Madden & Julian, 1971; Zhang, 2005). Its planetary-scale structure, intraseasonal time-scale, and slow eastward propagation at ~5 m s<sup>-1</sup> make this wave stand out from other forms of equatorial variability such as the equatorial waves (Kiladis et al., 2009). Recently, it has become clear that interactions between moisture, convection, radiation, and circulation are important for the dynamics of the MJO (Sobel et al., 2001; Raymond, 2001; Sobel & Maloney, 2013; Á. Adames & Kim, 2016; Gonzalez & Jiang, 2019; Á. Adames & Maloney, 2021; Ahmed, 2021; Wang & Sobel, 2021). These interactions can cause the dynamics of the MJO to significantly differ from those described by dry shallow water theory. Indeed, the MJO does not correspond to any of Matsuno's solutions (Matsuno, 1966).

Many theoretical models have been proposed to explain the MJO's features. These theories have been recently documented by Zhang et al. (2020) and Jiang et al. (2020). Among these theories, the moisture mode theory has arguably gained the most attention (Á. Adames & Maloney, 2021). In this theory, the evolution of moisture governs the evolution of the wave. The primary signatures of moisture modes are (a) a strong moisture tendency and (b) a weak temperature tendency (Á. Adames et al., 2019; Ahmed et al., 2021; Á. Adames & Maloney, 2021). The first condition manifests as a tight coupling between moisture and precipitation. The second condition ensures that the weak temperature gradient approximation (WTG; Sobel et al., 2001) is the dominant column energy balance. These two conditions underpin the criteria proposed in Mayta et al. (2022) to classify different tropical systems. By using these criteria, Mayta and Adames (2023) found that the MJO over the Western Hemisphere does not satisfy the conditions to be a moisture mode. Other studies have also argued that the circumnavigating MJO signature—where it is weakly coupled with convection— agrees with the convectively-coupled Kelvin wave rather than a moisture mode (Sobel & Kim, 2012; Powell, 2017; Á. Adames et al., 2019; Emanuel, 2020; Ahmed et al., 2021). However, other studies have shown that the MJO's signature over the Indo-Pacific warm pool has the features of moisture modes (e.g., Myers & Waliser, 2003; Á. Adames & Kim, 2016; Kim et al., 2017; Á. Adames, 2017; Snide et al., 2022, among others).

These results give us the main scientific question of this study: Is the MJO a moisture mode? Is it possible that the MJO is a moisture mode only in some regions of the tropics? The structure of this paper is as follows: In

Section 2, we discuss the data and statistical methods used to explore moisture mode conditions associated with the MJO. In Section 3, we examine the leading thermodynamic properties and assess its consistency with moisture mode theory (Á. Adames et al., 2019; Ahmed et al., 2021; Mayta et al., 2022). In Section 4, we will employ a recent theory by Ahmed et al. (2021) to show that the MJO exhibits moisture mode behavior in regions where the atmosphere favors this behavior near the planetary scales. A concluding discussion is offered in Section 5.

#### 2. Data and Methods

### 2.1. Satellite CLAUS $T_b$ and Reanalysis Data Set

Satellite-observed brightness temperature  $(T_b)$  data were used as a proxy for convection. The satellite data is obtained from the Cloud Archive User System (CLAUS) (Hodges et al., 2000). Three-dimensional atmospheric fields, including zonal and meridional winds (u, v), pressure velocity  $(\omega)$ , specific humidity (q), temperature (T), diabatic heating rate  $(Q_1)$ , surface and top of the atmospheric radiative fluxes, surface sensible and latent heat fluxes (SH and LE), respectively), and precipitation (P) were obtained from the European Centre for Medium-Range Weather Forecasts ERA-5 reanalysis (ERA5; Hersbach et al., 2019). The ERA5 data set uses a  $1.0^{\circ}$  horizontal resolution grid, with four times daily analyses that match the CLAUS  $T_b$  data for the 36-year time period 1984 through 2015. We focused on MJO activity during the extended boreal winter season (November to April).

#### 2.2. Field Campaign Data

To further analyze the moist process in the MJO and verify the accuracy of reanalysis data, we used observed data from three field campaigns around the tropical belt: (a) Over the Indian Ocean, we use data from the Dynamics of the Madden-Julian Oscillation (DYNAMO) field campaign, conducted from October 2011 through March 2012 (Yoneyama et al., 2013). We used data from the northern sounding array (NSA) averages from observations, located in the central equatorial Indian Ocean for a 3-month period from 10 October through 31 December 2011. The sounding array data set was quality-controlled and bias corrected to create a DYNAMO legacy data set (Ciesielski et al., 2014). (b) In the Western Pacific, we used data collected during intensive operating period (IOP) of TOGA-COARE for a 4-month period from 1 November through 28 February 1993. A detailed description of sounding stations and quality control procedures for TOGA-COARE was documented in Webster and Lukas (1992). All calculations we present are average vertical profiles for grid points within Intensive Flux Array (IFA), which is an array of sounding stations centered near 2°S, 155°E (Figure 1). (c) For tropical South America, the Observations and Modeling of the Green Ocean Amazon (GoAmazon 2014/15) are used. The field campaign was carried out in central Amazonia, Brazil for a 2-year time period from 1 January 2014 through 31 December 2015. For this study, we make use of the constrained variational analysis product for GoAmazon (VARANAL; Tang et al., 2016). VARANAL is derived from the ECMWF analysis fields and Atmospheric Radiation Measurement's (ARM) observations during GoAmazon 2014/15 using the constrained variational analysis proposed in Zhang and Hendon (1997). This product assimilates the top of the atmosphere and surface observations to produce thermodynamic budgets. The surface observations assimilated include surface radiative, latent, and sensible heat fluxes and precipitation from the System for the Protection of Amazonia (SIPAM) radar. Additional details about VARANAL products during GoAmazon 2014/15 are found in Tang et al. (2016).

Finally, we make use of the all-season OLR MJO index (OMI; Kiladis et al., 2014) as a measure of MJO activity. This index represents the convection MJO features and is commonly used to track the life cycle of an MJO event.

## 2.3. Linear Regression

Thermodynamic anomaly fields associated with the MJO are obtained by projecting raw ERA5 data at each grid point onto the associated first principal component (OMI1) time series. Then, all fields are scaled to one standard deviation OMI1 perturbation as made in previous studies (e.g., Mapes et al., 2006; Á. Adames et al., 2021; Mayta & Adames, 2021; Snide et al., 2022). The same approach is applied to data from campaigns. The area-average of filtered  $T_b$  or data at the same grid base point of the observations is used to calculate regressions instead. The statistical significance of these results is then assessed based on the two-tailed Student's t-test. This method takes into account the correlation coefficients and an effective number of independent samples (degrees of freedom) based on the decorrelation timescale (Livezey & Chen, 1983).

19448007, 2023, 15, Downloaded from https://agupubs.onlinelibrary.wiley.com/doi/10.1029/2023GL103002 by University Of Wisconsin - Madison, Wiley Online Library on [24.01/2024]. See the Terms and Conditions

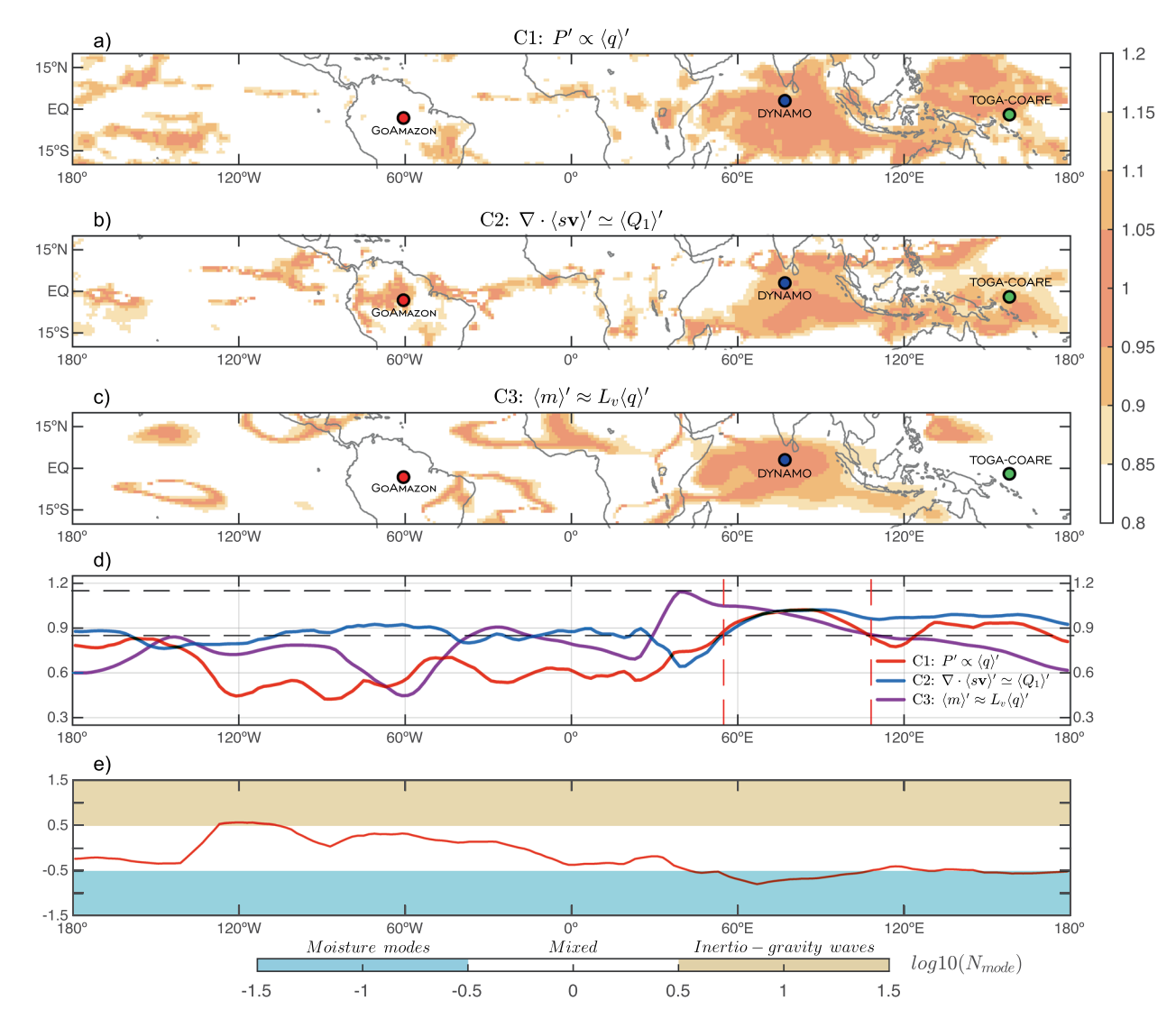


Figure 1. Geographical variations of the moisture mode criteria. Maps of (a) P' versus  $\langle q \rangle'$ , (b)  $\nabla \cdot \langle s v \rangle'$  versus  $\langle Q_1 \rangle'$ , and (c)  $\langle m \rangle'$  versus  $L_v \langle q \rangle'$ . Anomalies are obtained by projecting ERA5 data at each grid point onto the associated first principal component (OMI1) time series. Panel (a) shows the correlation coefficient, and panels (b) and (c) are the slopes of the linear fitting. (d) Represents the average value of each criterion computed from 10°S to 10°N at each longitude. The gray dashed lines represent the same threshold used in panels (a) to (c). The red dashed lines indicate the longitude domain where the three criteria are satisfied. Panel (e) shows the geographical variation of the dimensionless  $N_{mode}$  parameter. Shadings represent base 10 logarithm of  $N_{mode}$ , where blue represents  $N_{mode}$  values categorized as moisture modes, yellow can be considered inertio-gravity waves, and white represents mixed systems. The location of the DYNAMO, TOGA-COARE, and GO-Amazon sites is indicated by blue, green, and red circles, respectively.

# 3. Moist Thermodynamics of the MJO

We will now examine three criteria first described by Ahmed et al. (2021), applied to the entire tropical belt. In Mayta et al. (2022), these criteria were modified to make them more suitable for their diagnosis in observational and reanalysis data. These criteria are:

(a) Criterion 1 (C1): The wave must exhibit a large moisture signature that is highly correlated with the precipitation anomalies

For the MJO to be considered a moisture mode, its signature in column water vapor ( $\langle q \rangle'$ ) must be large enough to explain the majority of the surface rainfall variance (P'), given the following relation,

$$P' \propto \langle q \rangle' \tag{1}$$

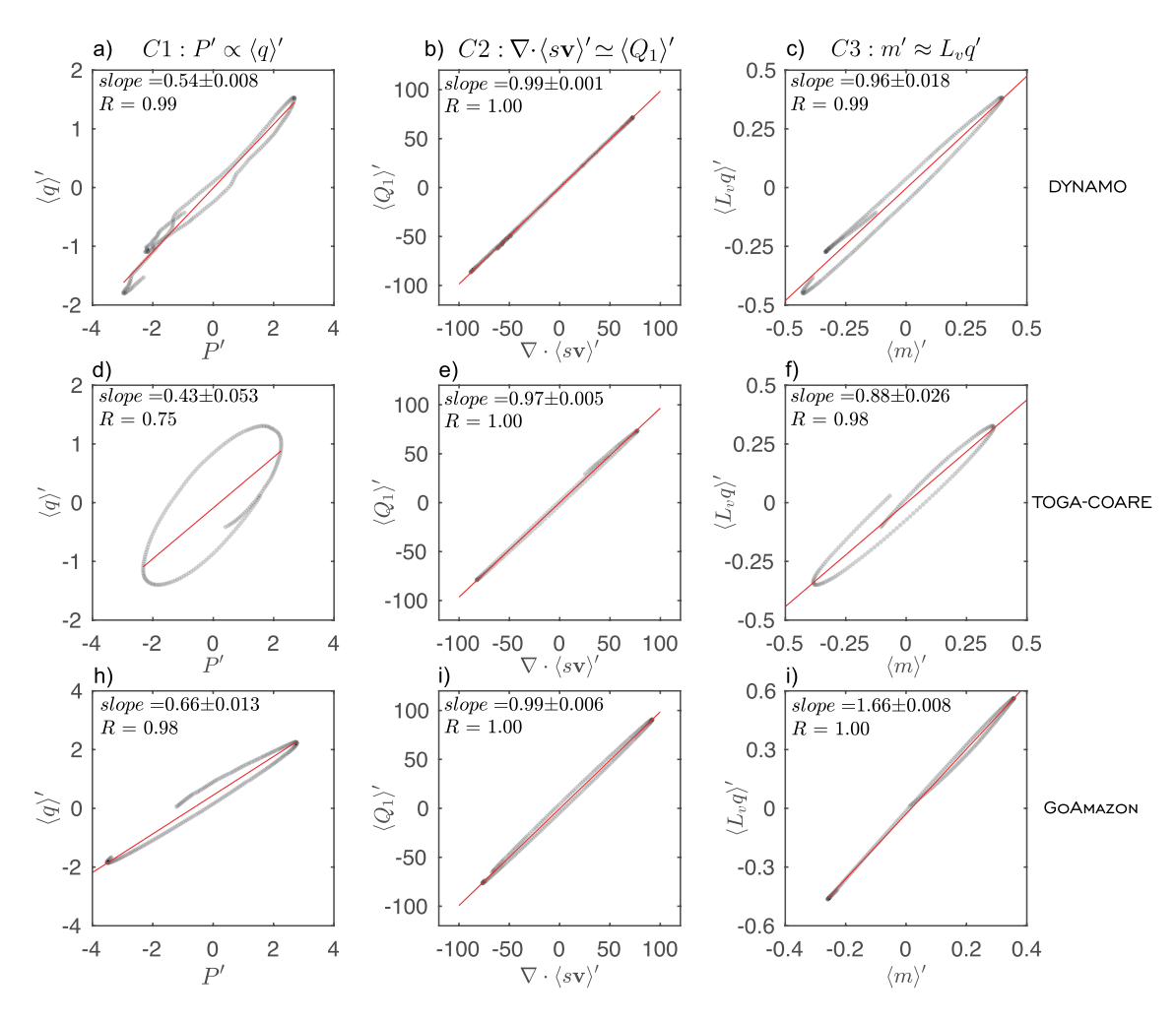


Figure 2. Scatterplots of P' versus  $\langle q \rangle'$  (first column),  $\nabla \cdot \langle s \mathbf{v} \rangle'$  versus  $\langle Q_1 \rangle'$  (second column), and  $\langle m' \rangle$  versus  $\langle L, q' \rangle$  (third column) for the DYNAMO (top panels), TOGA-COARE (middle panels), and GoAmazon (bottom panels), respectively. Anomalies are obtained by regressing all fields against the time series of the filtered  $T_b$  at the corresponding base point of the field campaign (See Figure 1). The linear least squares fit is shown as a solid red line. The slope of the linear fit and the correlation coefficient are shown in the top-left of each panel.

This results in a strong correlation ( $\sim$ 0.9 rounded) between P' and  $\langle q \rangle'$  (Mayta & Adames, 2023; Mayta et al., 2022). In this study,  $\langle \cdot \rangle \equiv 1/g \int_{surf.}^{top} (\cdot) dp$  denotes the mass-weighted vertical integral and primes (') represent intraseasonal anomalies.

We apply this criterion by constructing a scatterplot between P' and  $\langle q \rangle'$  at each grid point in the reanalysis (Figure 1a) and at the corresponding base point for the field campaign data (Figure 2). The correlations between P' and  $\langle q \rangle'$  from ERA5 are plotted in Figure 1a, and the latitudinal averages in Figure 1d. Results show that only over the Indo-Pacific warm pool region passes the first criterion, with correlations ranging close to  $\sim$ 1.0. An exception occurs around the Maritime Continent, where correlations are beneath 0.9. Interactions with the islands might cause correlations to diminish, possibly owing to the barrier effect of the Maritime Continent, where MJO propagation is often stalled or even ends around this region when convection is strong over the islands (Kim et al., 2014, 2017). Correlations decay drastically outside of the warm pool, from 150°W to 40°E, where the mean correlation value is of  $\sim$ 0.5 (Figure 1d).

When data from the field campaigns are analyzed instead, we see that a strong correlation between P' and  $\langle q \rangle'$  is seen for the DYNAMO data (Figure 2a). As the MJO moves away from the warm pool, correlations decrease as depicted in the TOGA-COARE data, where a correlation between P' and  $\langle q \rangle'$  is about  $\sim 0.75$  (Figure 2d). The cyclical appearance of the cloud of points is suggestive of a lead/lag relationship between the two fields, rather than an in-phase one. A high correlation of  $\sim 0.98$  (Figure 2h) is seen once again at the GoAmazon base point, in disagreement with ERA5.

(b) Criterion 2 (C2): The mode must be in weak temperature gradient (WTG) balance

WTG balance is the leading thermodynamic balance in the tropics (Sobel et al., 2001). This balance states that vertical dry static energy (DSE) advection approximately balances heating

$$\nabla \cdot \langle s\mathbf{v} \rangle' \simeq \langle Q_1 \rangle' \tag{2}$$

where  $s = C_p T + \phi$  is DSE,  $\mathbf{v} = u\mathbf{i} + v\mathbf{j}$  is the horizontal vector wind field,  $C_p = 1004 \text{ J kg}^{-1} \text{ K}^{-1}$  is the specific heat at constant pressure, and T is the temperature.  $\langle Q_1 \rangle' \simeq \langle Q_r \rangle' + L_v P' + SH'$  is the apparent heating rate and can be calculated from reanalysis and observations following Yanai and Johnson (1993), where  $Q_r$  is the radiative heating rate, SH is the surface sensible heat flux, and  $L_v$  represents the latent heat of vapourization  $(2.5 \times 10^6 \text{ J kg}^{-1})$ . To pass this criterion, the MJO must exhibit a slope of the linear least-square fit within the margin of  $\sim 0.9-1.1$  (rounded). This assumption implies that the residual between the two fields is roughly an order of magnitude smaller than the individual terms.

Figure 1b shows the value of the slope of the linear least-square fit at each grid point. We can see that the slope is ~1 from the Indian Ocean toward the Western Pacific. Regions over the mean climatological ITCZ position, including the Amazon basin, are also places where this criterion is satisfied. The meridionally-averaged values (Figure 1d) show that the criterion largely prevails from 50°E to 180°. Observations are also in agreement with reanalysis. Results show a high correlation between  $\nabla \cdot \langle s\mathbf{v} \rangle'$  and  $\langle Q_1 \rangle'$ , with a slope of ~0.99, ~0.97, and ~0.99 for DYNAMO, TOGA-COARE, and GoAmazon, respectively (Figures 2b, 2e and 2i).

(c) Criterion 3 (C3): Moisture must govern the distribution of moist static energy (MSE)

If the MJO is a moisture mode, moisture should be the main contributor to MSE, implying that

$$\langle m \rangle' \approx L_v \langle q \rangle'$$
 (3)

where  $m = s + L_v q$  is MSE. As in C2, a slope of the linear least-square fit within the margin of  $\sim 0.9-1.1$  (rounded) is needed to guarantee the balance of Equation 3. From Figure 1c, we see that the slope of the linear fit is  $\sim 1$  only over the Indian Ocean. According to the average values presented in Figure 1d (solid magenta line), this criterion is satisfied from 45°E to 130°E. Results from ERA5 can be verified with observations at different base points. From DYNAMO (Figure 2c) it is possible to see that the slope is about  $\sim 1$  over the Indian Ocean. The slope diminishes at the TOGA-COARE base point (0.88, Figure 2f), and completely falls outside the threshold over GoAmazon (1.66, Figure 2i).

(d) N<sub>mode</sub>

 $N_{mode}$  is a nondimensional number that quantifies the relative contribution of moisture and temperature to any convectively coupled wave. This parameter can be computed as in Á. Adames et al. (2019),

$$N_{mode} \simeq \frac{c_p^2 \tau}{c^2 \tau} \tag{4}$$

where c is the phase speed of a first baroclinic free gravity wave ( $c \simeq 50 \text{ ms}^{-1}$ ),  $c_p$  is the phase speed of the MJO,  $\tau_c = \langle q \rangle'/P'$  is the convective moisture adjustment time scale defined as the time precipitation takes to remove column moisture (Betts, 1986), and  $\tau = \lambda/c_p$  is the characteristic time-scale, with  $\lambda$  being the wavelength. When  $N_{mode} \ll 1$ , moisture governs the thermodynamics of the MJO, resulting in moisture modes; but if  $N_{mode} \gg 1$  the thermodynamics of a wave are predominantly driven by thermal fluctuations, resulting in gravity waves. When  $N_{mode} \approx 1$  the MJO will exhibit the behavior of both moisture mode and gravity wave.

Figure 1e shows the geographical variation of the base 10 logarithm of the dimensionless  $N_{mode}$  parameter. From Equation 4,  $\tau_c$  varies at each longitude (Figure S1a in Supporting Information S1),  $\tau$  is assumed to be 45 days, the average value throughout the tropics and  $c_p$  is computed for different regions (see Table S1 in Supporting Information S1). The zonal distribution of  $N_{mode}$  is in qualitative agreement with the three criteria discussed above. Values of  $N_{mode}$  smaller than 0.3 are observed exclusively from 60°E throughout 180°. The smallest value of  $N_{mode}$  is found over the Eastern Indian Ocean (60°E–90°E, Figure 1e), where the MJO propagates slowly at about ~4.1 m s<sup>-1</sup> (Table S1 in Supporting Information S1). In contrast, larger values of  $N_{mode}$  are observed over the Eastern Pacific, in a region where the wave propagates faster. These results show that  $N_{mode}$  is strongly modulated

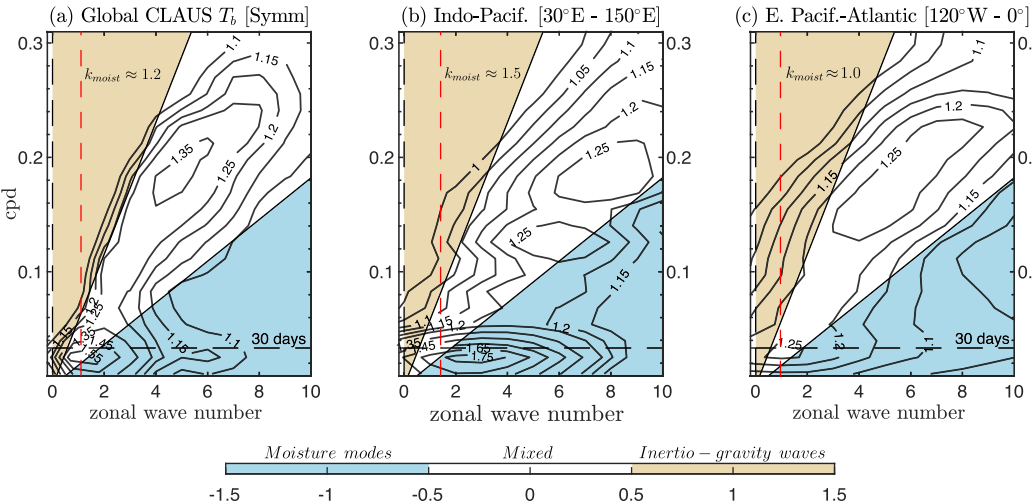


Figure 3. Wavenumber-frequency power spectrum (contours) of the symmetric component of CLAUS  $T_b$  calculated for (a) global [10°N–10°S, 0°–360°] and (b) Indo - Pacific [10°N–10°S, 30°E–150°E], and (c) East Pacific - Atlantic [10°N–10°S, 120°W–0°] and for the extended boreal winter (November-April). The functional form of the tapering window is the same as described in Wheeler and Kiladis (1999). Background spectra were estimated separately for the regional domain, using the smoothing procedure of Dias and Kiladis (2014). Contours are the ratio between raw  $T_b$  power and the power in a smoothed "red-noise" background exceeds 1.1, with intervals of 0.05. Shadings correspond to ranges of phase speed;  $c_p < 8.0 \text{ m s}^{-1}$  (blue) and  $c_p > 25.0 \text{ m s}^{-1}$  (yellow). Blue shading represents tropical systems that can be categorized as moisture modes, yellow can be considered inertio-gravity waves, and white represents mixed systems. Adapted from Á. Adames et al. (2019). The red dashed lines in all panels indicate the moisture mode cutoff wavenumber ( $k_{moist}$ ).

 $log_{10}(N_{mode})$ 

by the  $c_p$  of the wave rather than  $\tau_c$  and  $\tau$ , which means that a slower MJO propagation allows more time to eliminate temperature fluctuations, adjusting to WTG.

When all conditions are examined together, we conclude that the MJO is a moisture mode only over the eastern Indian Ocean (60°E to 110°E; Figure 1d). Elsewhere, it is not a moisture mode but rather exhibits mixed behavior (Mayta & Adames, 2023; Powell, 2017; Sobel & Kim, 2012), as will be discussed in the following section.

In order to objectively quantify the regional dependence of the moisture mode features of the MJO, the space-time spectra of  $T_b$  for the global and regional domains are computed, as shown in Figure 3: global ( $10^{\circ}\text{N}-10^{\circ}\text{S}$ ,  $0^{\circ}-360^{\circ}$ ), Indo - Pacific ( $10^{\circ}\text{N}-10^{\circ}\text{S}$ ,  $30^{\circ}\text{E}-150^{\circ}\text{E}$ ), and East Pacific - Atlantic ( $10^{\circ}\text{N}-10^{\circ}\text{S}$ ,  $120^{\circ}\text{W}-0^{\circ}$ ). More details about the calculation of regional spectra can be found in the figure caption. The wavenumber-frequency distribution of base 10 logarithm of  $N_{mode}$ , following a similar procedure of Á. F. Adames (2022), is depicted as shading. See also in Supporting Information S1 for a detailed calculation of  $N_{mode}$  spectrum. Areas shaded in blue are moisture modes. Each spectrum shows clear evidence of the differences in the intraseasonal time scale (time periods longer than 30 days). In the global and East Pacific-Atlantic domain, stronger power spectra are mainly concentrated in planetary wavenumbers  $k \approx 1-2$  (Figures 3a and 3c). According to the  $N_{mode}$  wavenumber-frequency spectra, a large portion of the intraseasonal signal in these regions is located in the mixed moisture-gravity wave regime (e.g., white region in Figure 3c). In the Indo-Pacific spectrum (Figure 3b), a wide range of zonal wavenumbers ( $k \approx 0-7$ ) are observed. The peaks are centered at wavenumbers k = 2-4, in a region where moisture modes are expected according to the  $N_{mode}$  spectrum.

# 4. The Moisture Mode Cutoff Wavenumber $(k_{moist})$

To better understand the differences in the spectral signal shown in Figure 3, we employ the linear theory of Ahmed et al. (2021) to assess whether the different behavior is the result of mean state differences. Their theory examined the dispersion relation of an MJO-like mode without assuming moisture mode a priori. They found the existence of a "moisture mode cutoff wavenumber" ( $k_{moist}$ ), which describes the wavenumber in which mixed systems [they refer to quasi-equilibrium modes] transition to moisture modes. Moisture mode behavior is found when  $k > k_{moist}$ , but if  $k < k_{moist}$  convection dries the troposphere before gravity waves are able to adjust

120°W

120°W

60°W

60°W

60°W

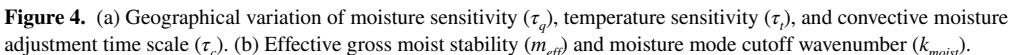
(a) Moisture and temperature sensitivity

10

 $\tau_q, au_t[days]$ 

0.2 0.15 0 120°E

120°E



toward WTG, and the waves behave as mixed moisture-gravity wave. Qualitatively,  $k_{moist}$  is the zonal wavenumber in which  $N_{mode} \approx 1$ , with  $N_{mode}$  being smaller than unity for larger values of k. The value of  $k_{moist}$  is determined from the following relation,

0°

vs. Moisture mode cutoff wavenumber  $[k_{moist}]$ 

60°E

60°E

$$k_{moist} \approx \frac{2}{c} \sqrt{\frac{m_{eff}(\tau_t + \tau_q)}{\tau_q^2 \tau_t}}$$
 (5)

where  $m_{eff}$  is the effective gross moist stability (GMS), defined as a measure of MSE export by convection and radiation per unit of heating (Inoue & Back, 2017; Inoue et al., 2020). A detailed derivation and scale analysis of Equation 5 is explained in Supporting Information S1. The terms  $\tau_t$  and  $\tau_q$  can be defined as a measure of the sensitivity of precipitation to temperature and moisture fluctuations. The values of  $\tau_t$  and  $\tau_q$  in Equation 5 are estimated as in Ahmed et al. (2020), where precipitation can be related to moisture and temperature by using a multiple linear regression model as follows,

$$P' = \frac{\langle q \rangle'}{\tau_q} - \frac{C_p}{L_v} \frac{\langle T \rangle'}{\tau_t} \tag{6}$$

Using Equation 6 and following Ahmed et al. (2021), we can also show that the convective adjustment  $\tau_c$  is a combination of  $\tau_t$  and  $\tau_a$ ,

$$\tau_c = \frac{\gamma_{qT} \tau_q \tau_t}{\gamma_{qT} \tau_t + \tau_q} \tag{7}$$

where  $\gamma_{qT} = -\frac{L_v(q)'}{C_p(T)'}$  is the ratio of moisture to temperature perturbations. Over the regions where the MJO is a moisture mode  $\gamma_{qT} \approx 10$  (e.g., Figure 2c), giving  $\tau_c \approx \tau_q$ ; that is, the convective adjustment time is determined by the moisture sensitivity (Figure 4a). For the Indo-Pacific warm pool region, we obtain an average value of the convective sensitivities  $\tau_t$  and  $\tau_q$  of about 12.5 and 24.3 hr. These values are longer than those used in Ahmed et al. (2021) because using time-filtered data always yields larger adjustment times since precipitating and non-precipitating times are convolved (Ahmed et al., 2020). Similar values are obtained outside the warm pool except near the prime meridian, where both  $\tau_q$  and  $\tau_t$  increase by nearly a factor of 3.

As Equation 5 indicates, the moisture mode cutoff wavenumber decreases with decreasing  $m_{eff}$ . We computed the value of  $m_{eff}$  from reanalysis for the entire tropical region (Figure 4b). For the MJO, we found an average value of  $m_{eff} \sim 0.05$  at nearly every longitude. When combining all these results together, we find that  $k_{moist}$  exhibits a near-constant value of  $\sim 1$  throughout the tropics (Figure 4b). Globally, the MJO signal strength is concentrated at planetary wavenumbers  $k \approx 1-2$ , falling within the mixed moisture-gravity part of the  $N_{moist}$  spectrum (Figure 3a). Over the Indian Ocean, the MJO signal is centered on wavenumbers larger than  $k_{moist}$ , consistent with the four

#### 5. Summary and Conclusions

On basis of four criteria to identify moisture modes proposed in previous works ( $\acute{A}$ . Adames et al., 2019; Ahmed et al., 2021; Mayta et al., 2022), we demonstrated that the MJO can be considered a moisture mode only over the Indian Ocean ( $60^{\circ}$ E to  $110^{\circ}$ E; Figure 1d). The results showed that it is because the MJO signal project primarily at higher wavenumbers in these regions. Over the Indian Ocean, MJO can also show characteristics of moisture modes even at planetary scales (except wavenumber 1), consistent with the  $N_{mode}$  spectrum (Figure 3b).

Outside the Indo-Pacific warm pool, the moisture mode criteria were not satisfied in either the reanalysis or observations (Figures 1 and 2). Instead, a large fraction of the MJO signal was observed in wavenumbers  $k \sim 1-2$ , falling into the mixed moisture-gravity wave part of the  $N_{mode}$  spectrum (Figures 3a and 3c). Under these conditions, WTG balance is not achieved at the MJO scale, and temperature and moisture fluctuations play comparable roles. These results are in agreement with previous works that posited that the planetary-scale component of the MJO is not a moisture mode (Powell, 2017; Á. Adames et al., 2019; Ahmed et al., 2021; Chen, 2022; Mayta & Adames, 2023). In other words, the circumnavigating MJO component outside of the warm pool exhibits features that are more akin to a Kelvin wave (e.g., Sobel & Kim, 2012).

The results of this study have several implications. First, more theoretical work must be done to understand how a zonally-varying mean state affects the MJO (e.g., Tulich and Kiladis (2021); Rushley et al. (2023)). These results can also help us understand the scale selection mechanism of the MJO, which is likely not determined by moisture mode processes (Rostami et al., 2022). Furthermore, the transition from moisture mode to a mixed wave should be examined further, especially with more GCMs. While not discussed here, this transition may help us further understand the Maritime Continent barrier effect (Zhang & Ling, 2017), and the MJO-QBO connection (Son et al., 2017), both of which occur in the region where the MJO begins to exhibit a transition from a moisture mode to a mixed system. Lastly, it is curious that MJO initiation occurs in the region where thermodynamic variations in the wave are dominated by moisture. It is possible that deviations from WTG balance play an important role in exciting moisture modes, as Snide et al. (2022) posited. All of these outstanding questions may be fruitful directions for future research.

## **Data Availability Statement**

The data set used in this study are available at ECWF (ERA5; https://doi.org/10.24381/cds.adbb2d47), the Atmospheric Radiation Measurement (ARM) program archive (VARANAL; https://iop.archive.arm.gov/arm-iop/0eval-data/xie/scm-forcing/iop\_at\_mao/GOAMAZON/2014-2015/) [registration is required to access data], TOGA-COARE data set are available at https://data.eol.ucar.edu/dataset/dsproj?TOGA\_COARE, and the interpolated CLAUS  $T_b$  data is available at https://catalogue.ceda.ac.uk/uuid/ce476101711ce73107c9e-90265ec6d9a. DYNAMO NSA array averages from observations data (Version 3a) are available at http://johnson.atmos.colostate.edu/dynamo/. The OMI index is available at https://psl.noaa.gov/mjo/mjoindex/.

#### Acknowledgments

VM and ÁFAC are supported by NOAA Grant NA22OAR4310611. VM and ÁFAC were also supported by NSF CAREER Grant 2236433 and by the University of Wisconsin startup package. The contents of the manuscript were significantly improved after conversations with Fiaz Ahmed.

## References

Adames, Á. (2017). Precipitation budget of the Madden–Julian Oscillation. *Journal of the Atmospheric Sciences*, 74(6), 1799–1817. https://doi.org/10.1175/JAS-D-16-0242.1

Adames, Á., & Kim, D. (2016). The MJO as a dispersive, convectively coupled moisture wave: Theory and Observations. *Journal of the Atmospheric Sciences*, 73(3), 913–941. https://doi.org/10.1175/JAS-D-15-0170.1

Adames, Á., Kim, D., Clark, S. K., Ming, Y., & Inoue, K. (2019). Scale analysis of moist thermodynamics in a simple model and the relationship between moisture modes and gravity waves. *Journal of the Atmospheric Sciences*, 76(12), 3863–3881. https://doi.org/10.1175/IAS-D-19-01211

Adames, Á., & Maloney, E. D. (2021). Moisture mode theory's contribution to advances in our understanding of the Madden-Julian Oscillation and other tropical disturbances. *Current Climate Change Reports*, 7(2), 72–85. https://doi.org/10.1007/s40641-021-00172-4

Adames, Á., Powell, S. W., Ahmed, F., Mayta, V. C., & Neelin, J. D. (2021). Tropical precipitation evolution in a buoyancy-budget framework. Journal of the Atmospheric Sciences, 78(2), 509–528. https://doi.org/10.1175/JAS-D-20-0074.1

Adames, Á. F. (2022). The basic equations under weak temperature gradient balance: Formulation, scaling, and types of convectively-coupled motions. *Journal of the Atmospheric Sciences*, 79(8), 2087–2108. https://doi.org/10.1175/JAS-D-21-0215.1

Ahmed, F. (2021). The MJO on the equatorial beta plane: An eastward-propagating Rossby wave induced by meridional moisture advection. Journal of the Atmospheric Sciences, 78(10), 3115–3135. https://doi.org/10.1175/JAS-D-21-0071.1

- Ahmed, F., Adames, Á. F., & Neelin, J. D. (2020). Deep convective adjustment of temperature and moisture. *Journal of the Atmospheric Sciences*, 77(6), 2163–2186. https://doi.org/10.1175/JAS-D-19-0227.1
- Ahmed, F., Neelin, J. D., & Adames, Á. F. (2021). Quasi-equilibrium and weak temperature gradient balances in an equatorial beta-plane model. Journal of the Atmospheric Sciences, 78(1), 209–227. https://doi.org/10.1175/JAS-D-20-0184.1
- Betts, A. K. (1986). A new convective adjustment scheme. Part I: Observational and theoretical basis. Quarterly Journal of the Royal Meteorological Society, 112(473), 677–691. https://doi.org/10.1002/qi.49711247307
- Chen, G. (2022). The amplification of Madden–Julian Oscillation boosted by temperature feedback. *Journal of the Atmospheric Sciences*, 79(1), 51–72. https://doi.org/10.1175/JAS-D-21-0146.1
- Ciesielski, P. E., Yu, H., Johnson, R. H., Yoneyama, K., Katsumata, M., Long, C. N., et al. (2014). Quality-controlled upper-air sounding data-set for dynamo/Cindy/Amie: Development and corrections. *Journal of Atmospheric and Oceanic Technology*, 31(4), 741–764. https://doi.org/10.1175/itech-d-13-00165.1
- Dias, J., & Kiladis, G. N. (2014). Influence of the basic state zonal flow on convectively coupled equatorial waves. *Geophysical Research Letters*, 41(19), 6904–6913. https://doi.org/10.1002/2014GL061476
- Emanuel, K. (2020). Slow modes of the equatorial waveguide. Journal of the Atmospheric Sciences, 77(5), 1575–1582. https://doi.org/10.1175/ias-d-19-0281.1
- Gonzalez, A. O., & Jiang, X. (2019). Distinct propagation characteristics of intraseasonal variability over the tropical west Pacific. *Journal of Geophysical Research: Atmospheres*, 124(10), 5332–5351. https://doi.org/10.1029/2018JD029884
- Hersbach, H., Bell, W., Berrisford, P., Horányi, A., Muñoz-Sabaters, J. J., Nicolas, J., et al. (2019). Global reanalysis: Goodbye ERA-interim (pp. 17–24). hello ERA5. https://doi.org/10.21957/vf291hehd7
- Hodges, K. I., Chappell, D. W., Robinson, G. J., & Yang, G. (2000). An improved algorithm for generating global window brightness temperatures from multiple satellite infrared imagery. *Journal of Atmospheric and Oceanic Technology*, 17(10), 1296–1312. https://doi.org/10.1175/1520-0426(2000)017<1296:aiafgg>2.0.co;2
- Inoue, K., Adames, Á. F., & Yasunaga, K. (2020). Vertical velocity profiles in convectively coupled equatorial waves and MJO: New diagnoses of vertical velocity profiles in the wavenumber-frequency domain. *Journal of the Atmospheric Sciences*, 77(6), 2139–2162. https://doi.org/10.1175/JAS-D-19-0209.1
- Inoue, K., & Back, L. E. (2017). Gross moist stability analysis: Assessment of satellite-based products in the GMS plane. *Journal of the Atmospheric Sciences*, 74(6), 1819–1837. https://doi.org/10.1175/JAS-D-16-0218.1
- Jiang, X., Adames, n. F., Kim, D., Maloney, E. D., Lin, H., Kim, H., et al. (2020). Fifty years of research on the Madden-Julian Oscillation: Recent progress, challenges, and Perspectives. *Journal of Geophysical Research: Atmospheres*, 125(17), e2019JD030911. https://doi.org/10.1029/2019JD030911
- Kiladis, G. N., Dias, J., Straub, K. H., Wheeler, M. C., Tulich, S. N., Kikuchi, K., et al. (2014). A comparison of OLR and circulation-based indices for tracking the MIO. Monthly Weather Review, 142(5), 1697–1715. https://doi.org/10.1175/MWR-D-13-00301.1
- Kiladis, G. N., Wheeler, M. C., Haertel, P. T., Straub, K. H., & Roundy, P. E. (2009). Convectively coupled equatorial waves. Reviews of Geophysics, 47(2), RG2003. https://doi.org/10.1029/2008rg000266
- Kim, D., Kim, H., & Lee, M.-I. (2017). Why does the MJO detour the Maritime Continent during austral summer? Geophysical Research Letters, 44(5), 2579–2587. https://doi.org/10.1002/2017GL072643
- Kim, D., Kug, J.-S., & Sobel, A. H. (2014). Propagating versus nonpropagating Madden–Julian Oscillation events. *Journal of Climate*, 27(1), 111–125. https://doi.org/10.1175/JCLI-D-13-00084.1
- Livezey, R. E., & Chen, W. Y. (1983). Statistical field significance and its determination by Monte Carlo techniques. *Monthly Weather Review*, 111(1), 46–59. https://doi.org/10.1175/1520-0493(1983)111<0046:sfsaid>2.0.co;2
- Madden, R. A., & Julian, P. R. (1971). Detection of a 40-50-day oscillation in the zonal wind in the tropical Pacific. *Journal of the Atmospheric Sciences*, 29(5), 1109–1123. https://doi.org/10.1175/1520-0469(1971)028<0702:doadoi>2.0.co;2
- Mapes, B., Tulich, S., Lin, J., & Zuidema, P. (2006). The mesoscale convection life cycle: Building block or prototype for large-scale tropical waves? *Dynamics of Atmospheres and Oceans*, 42(1), 3–29. https://doi.org/10.1016/j.dynatmoce.2006.03.003
- Matsuno, T. (1966). Quasi-geostrophic motions in the equatorial area. *Journal of the Meteorological Society of Japan*, 44(1), 25–43. https://doi.org/10.2151/jmsi1965.44.1\_25
- Mayta, V. C., & Adames, A. F. (2021). Two-day westward-propagating inertio-gravity waves during GoAmazon. *Journal of the Atmospheric Sciences*, 78(11), 3727–3743. https://doi.org/10.1175/JAS-D-20-0358.1
- Mayta, V. C., & Adames, A. F. (2023). Moist thermodynamics of convectively coupled waves over the western hemisphere. *Journal of Climate*, 36(9), 1–36. https://doi.org/10.1175/JCLI-D-22-0435.1
- Mayta, V. C., Adames, Á. F., & Ahmed, F. (2022). Westward-propagating moisture mode over the tropical western hemisphere. Geophysical Research Letters, 49(6), e2022GL097799. https://doi.org/10.1029/2022gl097799
- Myers, D. S., & Waliser, D. E. (2003). Three-dimensional water vapor and cloud variations associated with the Madden–Julian Oscillation during northern hemisphere winter. *Journal of Climate*, 16(6), 929–950. https://doi.org/10.1175/1520-0442(2003)016<0929:tdwvac>2.0.co;2
- Powell, S. W. (2017). Successive MJO propagation in MERRA-2 reanalysis. Geophysical Research Letters, 44(10), 5178–5186. https://doi.org/10.1002/2017GL073399
- Raymond, D. J. (2001). A new model of the Madden–Julian Oscillation. Journal of the Atmospheric Sciences, 58(18), 2807–2819. https://doi.org/10.1175/1520-0469(2001)058(2807;ANMOTM)2.0.CO;2
- Rostami, M., Zhao, B., & Petri, S. (2022). On the genesis and dynamics of Madden–Julian oscillation-like structure formed by equatorial adjustment of localized heating. *Quarterly Journal of the Royal Meteorological Society*, 148(749), 3788–3813. https://doi.org/10.1002/gi.4388
- Rushley, S. S., Kang, D., Kim, D., An, S.-I., & Wang, T. (2023). MJO in different orbital regimes: Role of the mean state on the MJO's amplitude during boreal winter. *Journal of Climate*, 36(13), 1–41. https://doi.org/10.1175/JCLI-D-22-0725.1
- Snide, C. E., Adames, Á. F., Powell, S. W., & Mayta, V. C. (2022). The role of large-scale moistening by adiabatic lifting in the Madden–Julian Oscillation convective onset. *Journal of Climate*, 35(1), 269–284. https://doi.org/10.1175/JCLI-D-21-0322.1
- Sobel, A., & Kim, D. (2012). The MJO-Kelvin wave transition. *Geophysical Research Letters*, 39(20), 1–5. https://doi.org/10.1029/2012GL053380 Sobel, A., & Maloney, E. (2013). Moisture modes and the eastward propagation of the MJO. *Journal of the Atmospheric Sciences*, 70(1), 187–192. https://doi.org/10.1175/JAS-D-12-0189.1
- Sobel, A., Nilsson, J., & Polvani, L. M. (2001). The weak temperature gradient approximation and balanced tropical moisture waves. *Journal of the Atmospheric Sciences*, 58(23), 3650–3665. https://doi.org/10.1175/1520-0469(2001)058(3650:TWTGAA)2.0.CO;2
- Son, S.-W., Lim, Y., Yoo, C., Hendon, H. H., & Kim, J. (2017). Stratospheric control of the Madden–Julian Oscillation. *Journal of Climate*, 30(6), 1909–1922. https://doi.org/10.1175/jcli-d-16-0620.1



# **Geophysical Research Letters**

- 10.1029/2023GL103002
- Tang, S., Xie, S., Zhang, Y., Zhang, M., Schumacher, C., Upton, H., et al. (2016). Large-scale vertical velocity, diabatic heating and drying profiles associated with seasonal and diurnal variations of convective systems observed in the GoAmazon2014/5 experiment. Atmospheric Chemistry and Physics, 16(22), 14249–14264. https://doi.org/10.5194/acp-16-14249-2016
- Tulich, S. N., & Kiladis, G. N. (2021). On the Regionality of moist kelvin waves and the MJO: The critical role of the background zonal flow. Journal of Advances in Modeling Earth Systems, 13(9), e2021MS002528. https://doi.org/10.1029/2021MS002528
- Wang, S., & Sobel, A. H. (2021). A unified moisture mode theory for the Madden Julian Oscillation and the boreal summer intraseasonal oscillation. *Journal of Climate*, 1–71.
- Webster, P. J., & Lukas, R. (1992). TOGA COARE: The coupled ocean-atmosphere response experiment. Bulletin of the American Meteorological Society, 73(9), 1377–1416. https://doi.org/10.1175/1520-0477(1992)073\(\)\(1377:TCTCOR\(\)\(2.0.CO;\)\(2)
- Wheeler, M., & Kiladis, G. (1999). Convectively-coupled equatorial waves: Analysis of clouds in the wavenumber-frequency domain. *Journal of the Atmospheric Sciences*, 56(3), 374–399. https://doi.org/10.1175/1520-0469(1999)056<0374:ccewao>2.0.co;2
- Yanai, M., & Johnson, R. (1993). Impacts of cumulus convection on thermodynamic fields. In K. A. Emanuel & D. J. Raymond (Eds.), The representation of cumulus convection in numerical models (pp. 39–62). Meteorological Monographs. https://doi.org/10.1007/978-1-935704-13-3\_4
- Yoneyama, K., Zhang, C., & Long, C. N. (2013). Tracking pulses of the Madden–Julian Oscillation. Bulletin of the American Meteorological Society, 94(12), 1871–1891. https://doi.org/10.1175/BAMS-D-12-00157.1
- Zhang, C. (2005). Madden-julian Oscillation. Reviews of Geophysics, 43(2), 1–36. https://doi.org/10.1029/2004rg000158
- Zhang, C., Adames, Á. F., Khouider, B., Wang, B., & Yang, D. (2020). Four theories of the Madden-Julian Oscillation. *Reviews of Geophysics*, 58(3), e2019RG000685. https://doi.org/10.1029/2019RG000685
- Zhang, C., & Hendon, H. H. (1997). Propagating and standing components of the intraseasonal oscillation in tropical convection. *Journal of the Atmospheric Sciences*, 54(6), 741–752. https://doi.org/10.1175/1520-0469(1997)054<0741:pascot>2.0.co;2
- Zhang, C., & Ling, J. (2017). Barrier effect of the indo-Pacific maritime continent on the MJO: Perspectives from tracking MJO precipitation. Journal of Climate, 30(9), 3439–3459. https://doi.org/10.1175/jcli-d-16-0614.1